Risk-Based Approach – Domino Effect and Escalation Triggered by Fragments

Projectile Impact Analysis

An ioMosaic White Paper

Jordi Dunjó, Ph.D.

Marcel Amorós

Neil Prophet

Gene Gorski

Abstract

Fragment projection following vessel burst scenarios is a potential cause of domino effect and escalation in the Chemical Process Industry (CPI). This proposes a risk-based missile impact domino effect analysis based on current research and published literature. This approach is suitable for use in the quantitative risk-based assessment framework.

Table of Contents

Appendices

Appendix I: Graphical Representation of Reference Fragmentation Patterns

Appendix II: Graphical Representation of Reference Fragment Shapes

Appendix III: Analytical Expression of Fragment Trajectory

List of Tables

List of Figures

Introduction

Fragment projection is usually caused by internal explosions (physical explosions, confined explosions, BLEVEs, runaway reactions) resulting in the catastrophic failure of vessels that transfer of part of the explosion energy to the projected fragments. Fragments may be projected very far from the damaged vessel (up to more than 1 km). Internal explosions have the potential to trigger secondary accidents causing the loss of integrity of the target vessel. When a fragment hits a target vessel, it may perforate the vessel, embed itself into the vessel, or ricochet. Therefore, the target can be damaged either by penetration or by plastic collapse **[1]**.

Catastrophic Vessel Failure

Catastrophic failures of process vessels may result in fragment projection and potentially cause worker injury/fatalities, asset damage and escalation events (domino effect). The fragment projection is usually coupled with the release of the vessel contents and the available internal energy at the Time To Failure (TTF):

- The available internal energy at TTF can result in a rise of blast waves and high-velocity fragments which can become missiles that propelled for long distances and hit objects in their trajectory. The available internal energy provides a source of fragmentation energy for the shell, resulting in kinetic energy imparted to contents that create fragments and blast wave energy. This process is not reversible as some internal energy will be dissipated as turbulence and heat transferred to the surroundings. Consequently, the prediction of the TTF and associated conditions such as the mass remaining in the vessel, phase, liquid level, pressure, temperature, mixture composition, are required parameters predicting the available internal energy in the vessel. Detailed criteria on how to predict the TTF and associated conditions can be found in references **[2]**, **[3]** and **[4]**.

- The release of the vessel contents can cause scenarios such as fireballs, vapor cloud explosions, flash fires and toxic dispersion, depending on the characteristics of the materials. Details of these different outcomes and associated effects to people (individual and societal risk characterization), to occupied buildings and to process equipment which could result in a domino effect, can be found in references **[5]** to **[14]**.

State-of-the-Art of Fragment Projection

Most of fragment projection studies assessed the probability of fragment impact. Less attention was dedicated to the conditional probability of damage given the impact, as it was usually assumed equal to one, indicating that damage always follows the impact [1].

The early work on the topic was mainly based on direct statistical analysis of accident data [15], [16]. The initial fragment velocity was calculated as a function of the explosion energy [15], [17] and associated conditions at the TTF. Fragment mass and number are also relevant to calculate the projection distance and to assess the energy received by each fragment. Other important parameters are the projection angles, for which a uniform distribution is assumed. The probability of impact was assessed as a function of distance and average kinetic energy received by the fragments.

More recently, a probabilistic method based on Monte Carlo simulations for the assessment of fragment impact probability was developed [18], [19]. The fragment trajectories are described by the basic equation of motion, but the critical parameters were discussed in detail. A simplified model for the assessment of the impact probability of fragments was developed [20]. The improved model is specifically aimed at the assessment of fragment impact probability on a target vessel. The model calculates the instantaneous velocity of fragments as a function of the angle of departure.

The range of departure angles leading to fragment impact is then calculated based on target distances and geometry. The probability of impact is assessed as the integral of the probability distribution function assumed for the projection angles in polar coordinates.

Studies based on the analysis of a database of 143 accidents where vessel fragmentation and fragment projection occurred provided statistical correlations on fragmentation patterns with respect to vessel features [21], on the drag factors and expected number of fragments generated [22] and on the probability distribution functions for the initial projection angles [23]. The overall approach resulting from this set of publications was recently applied to the detailed analysis of the 1993 refinery accident in Milazzo, Italy [24]. The accident characteristics were found to be consistent with the results of the modelling approach and the accident consequences resembled model consequences having a higher probability.

The development of 3D simulators allowed the use of improved Monte Carlo simulations to assess the probability of fragment impingement in a 3D environment **[25]**. Several improvements with respect to previous studies were introduced in this model: (1) a non-uniform probability for the fragment initial direction was assumed and (2) a separate model for fragment penetration in metal enclosures as a function of the fragment speed and mass was applied. The penetration model calculated the penetration probability of fragments in the metal wall, which was considered as a rigid object. The penetration model was adequate only for small fragments having a high velocity at the instant of the impact.

Based on the work on **[19]**, **[20]** and **[21]**, a procedure for the calculation of fragment impact probability was developed based on Monte Carlo simulations and a new methodology for the calculation of expansion energy and of the initial fragment velocity was presented **[26]**. The model identifies all the possible targets based on the maximum fragment projection distance.

From current available models for fragment impact characterization, it may be concluded that further work is needed to improve the available models. The low number of escalation accidents caused by fragment impact and the very high number of parameters that may affect fragment impact and damage, hindered the development and validation of vulnerability models such as probit analysis. However, the work developed in references **[20]**, **[21]**, **[22]** and **[23]** provides a systematic approach to evaluate fragment impact probability, which is valid for application in the quantitative risk-based assessment framework.

Proposed Risk-Based Approach Highlights

Based on the state-of-the-art of damage due to fragment impact, an approach is proposed for the assessment of the expected number and drag factor of fragments generated in the collapse of a vessel due to internal pressure. The analysis of a database reporting data on 143 vessel fragmentation events provided identification of a limited number of fragment reference shapes. The correlation of fragment reference shapes to the vessel credible fragmentation patterns supported the assessment of the expected number and general shape of fragments generated. Starting from the fragment reference shapes, simplified functions for drag factor calculation were developed, based on few geometrical parameters of the damaged vessel. The probabilistic models for the expected shape and number of fragments with the simplified drag factor functions constitute an important input for fragment trajectories in the quantitative risk-based assessments. This paper strictly follows criteria and data

developed in references **[20]**, **[21]**, **[22]** and **[23]**, which require the characterization of the following tasks once a vessel burst scenario has been identified:

- Estimation of the fragment initial velocity
- Identification of reference fragmentation patterns of process equipment
- Evaluation of fragment shapes and associated drag factors
- Estimation of probabilities of fragment escalation

Explosions Leading to Fragment Projection

Table 01 lists different primary scenarios that may lead to fragment projection.

Table 01: Explosions Leading to Fragment Projection

Explosion	Description
Fired BLEVE	Catastrophic failure of a vessel containing a liquid at temperature above its boiling temperature at atmospheric pressure, due to an external fire.
Unfired BLEVE	Sudden loss of containment of a vessel containing a liquid at temperature above its boiling temperature at atmospheric pressure, not due to an external fire.
Physical	Catastrophic failure of a vessel containing a compressed gas phase and/or a nonboiling liquid, due to an internal pressure increase not caused by fire or chemical reactions.
Confined	Catastrophic vessel failure due to an internal pressure increase caused by the unwanted combustion of gases, vapors, or dust inside the vessel.
Runaway	Catastrophic vessel failure due to an internal pressure increase caused by the loss of control of a chemical reaction.

Based on the characteristics of each explosion (such as pressure, temperature and stress rise), fracture mechanics and dynamics can be predicted, as well as the associated fragment properties (low or high fragment number crack arrest). Additionally, important outlines on the model of fragmentation may be drawn considering the influence of the vessel shape on the crack propagation.

For fragment projection to occur, the crack must propagate along the vessel surface to lead to the separation of at least one fragment that could project. Otherwise, a simple breach is created in the shell allowing the release of the vessel content, but without the generation of missiles. The analysis of past accident data **[21]** is summarized in **Table 02**.

Table 02: Probability of Fragment Generation [21]

Explosion	Probability of Fragment Generation; P_{CP} [-]
Fired BLEVE Unfired BLEVE Physical Explosion	0.9
Confined Explosion Runaway Reaction	1

Fragment Initial Velocity

When the explosion occurs at the TTF, the key consequence modeling parameters **[5]**, **[6]** are the available internal energy and the gas speed of sound. Several models in the literature evaluate the initial fragment velocity. The underlying purpose of these is to evaluate the fraction of the internal energy which is transferred to the fragments as kinetic energy during vessel failure. Some methods consider that all or almost all the internal energy available is transferred as kinetic energy to the fragments. Other definitions prescribe that the fragments will receive only a part of the internal energy, based on experimental observations. These methods are applicable to all types of vessels bursts, except to vessels filled with energetic materials **[22]**.

A ballistic model to retrofit data from the investigation of past accidents was developed and illustrated in reference **[20]**. The analysis suggested that a single mean value of the initial velocity of projection is sufficient to estimate the initial projection velocity of the fragments. The use of a kinetic energy model was found sufficiently precise for BLEVEs and mechanical explosions. In the case of BLEVE accidents involving Liquefied Petroleum Gas (LPG) vessels, the analysis showed that an average value of about 4% of the explosion energy was transferred to the fragments as kinetic energy. Other cited work in reference **[28]** provided a mean value of 5.77% and values between 4% and 6%; thus, a 5% seems to be a reasonable default value.

Confined explosions and runaway reactions also have been analyzed for predicting the initial velocity of fragments. The Baker Model **[27]** provided the best results when evaluating these explosions as confirmed in references **[20]** and **[28]**. **Table 03** provides criteria and guidance (**[20]**, **[28])** for models to be used for initial velocity estimations as a function of type of explosion.

Table 03: Models for the Initial Velocity of Fragments

Explosion	Initial Velocity Model	Equation ID
Fired/Unfired BLEVE Mechanical Explosion	$u = \sqrt{\alpha \cdot \left[\dfrac{2E_I}{M_V}\right]}$	**Equation 01**
Confined Explosion Runaway Reaction	$P_S = (P - P_{atm}) \cdot V_V / (M_V a^2)$	**Equation 02**
	a. For Cylindrical Vessels: $\log(u_s) = 0.56 \cdot \log(P_s) + 0.23$	**Equation 03**
	b. For Spherical Vessels: $\log(u_s) = 0.60 \cdot \log(P_s) + 0.13$	**Equation 04**
	$u = K u_s a$	**Equation 05**

*Nomenclature:

u: fragment initial velocity; E_I: available internal energy in the vessel at TTF; α: fraction of E_I transferred to fragments as kinetic energy (0.05); M_V: mass of the vessel; P: internal pressure in the vessel at TTF; P_{atm}: atmospheric pressure; V_V: vessel internal volume; a_0: sound speed of the gas at TTF; P_S: scaled pressure; u_S: scaled fragment velocity; K: model constant; ($K = 1$ for equal fragments).

Therefore, all required parameters for the evaluation of u are given from an accurate consequence modeling of the explosion event if the kinetic model is applicable; i.e., E_I, P, V_V, M_V, a. If Baker model is applied, only P, M_V and V_V are required for estimating the initial fragment velocity.

Assessment of Fragment Characteristics

Reference Fragment Patterns

Based on primary scenarios involving vessel fragmentation as listed in **Table 01** and on the analysis of fracture mechanics fundamentals, ideal reference fragmentation patterns were defined as a function of vessel type **[21]**.

Limiting the number of reference fragmentation modes that are linked to accident scenario and vessel geometry allows for generating the expected fragment shape and quantity. This is the basis for the definition of parameters necessary for the description of fragment trajectory, such as the mass, velocity and drag factor.

Table 04 lists the set of reference fragmentation patterns identified for metallic vessels as published in references **[21]** and **[22]**. No distinction was made between horizontal and vertical cylindrical vessels. Three vessel types are addressed:

- **CV**: Cylindrical Vessel

- **SV**: Spherical Vessel

- **CR**: Cone-Roof Tank

The conditional probability of a fragmentation pattern (P_{FP}) to occur following vessel fragmentation can be evaluated by past accident data. **Table 05** lists the conditional probabilities obtained from the analysis of the accidental events recorded in a database and are collected in reference **[21]**. The reported in the table, show that a limited number of different fragmentation patterns were sufficient to describe the fragmentation modes of the 143 accidents.

Table 04: Reference Fragmentation Patterns [21, 22]

Pattern	Description
CV1	An axial fracture starts and propagates in two opposite directions. If the two tips do not meet (more probable), one fragment (the entire vessel) may be projected, but no detached piece is formed. No branching and no direction turn (no connections and no defects) should take place to obtain this pattern. The vessel may not be deformed (cylindrical fragment) or it may be flattened (plate fragment).
CV2	The fracture, likely to start in the axial direction, may turn in the circumferential direction due to stress field changes (bending or stress intensification near connections), or to defects. If the axial crack propagates on the tube-end and stops, a flattened tube-end may be generated.
CV3	Credible if the fracture starts on a pipe connection or if one of the two tube-ends impacts on a near object at the moment of the projection.
CV4	Credible if the fracture starts on a pipe connection or if one of the two tube-ends impact on a near object at the moment of the projection. The axial fractures on the tube-end could arrest originating flattened tube-ends.
CV5	An axial crack may propagate in circumferential direction in zones where a stress concentration (thickness change, supports and pipe connections), defects or weldings are present. It is highly probable that the circumferential cracks are located at the ends. The shell fragment is generally flattened during the flight.
CV6	The axial fracture on the tube-end may arrest originating a flattened tube-end.
CV7	A longitudinal fracture branches in various points, starting circumferential fractures. Credible only for brittle fracture mechanisms. The shell is separated in more than one fragment.
SV1	A fracture on a spherical vessel may propagate in all directions because it will always be subjected to the same stress. It is possible to have more than one crack starting point. The number of fragments tends to grow with the vessel volume (higher the volume of the sphere and higher the surface area) because there is a higher probability for the fracture to encounter defects or to acquire a sufficient kinetic energy for branching.
CR1	Fracture on a cone-roof vessel may propagate along the roof-shell edge. The pattern is highly probable since the edge is a zone of stress concentration.

*Appendix A.I graphically illustrates each fragment pattern considered.

Table 05: Probability of Fragmentation Pattern [21]

Explosion	Probability of Fragment Pattern; P_{FP} [-]								
	CV1	CV2	CV3	CV4	CV5	CV6	CV7	SV1	CR1
Fired BLEVE	-	0.59	0.12	-	0.29	-	-	1.0	-
Unfired BLEVE	-	0.67	0.08	0.13	0.08	0.04	-	1.0	-
Physical Explosion	-	0.67	0.08	0.13	0.08	0.04	-	1.0	-
Confined Explosion	-	0.9	-	-	-	-	0.10	-	1.0
Runaway Reaction	0.29	0.43	-	-	0.14	-	0.14	-	-

CV: Cylindrical Vessel; **SV**: Spherical Vessel; **CR**: Cone-Roof Tank

Risk-Based Approach – Domino Effect and Escalation Triggered by Fragments

Reference Shapes for Fragments

The same research can expand the applicability and use of the reference fragmentation patterns by associating the following parameters:

- Expected total number of fragments: N_{FT}

- Reference shape (**CE**, **PT**, **PL**, **PTE1**, **PTE2**, **SC**, **CR,** see **Table 06**)

- Number of fragments with the same shape: N_{FS}

- Conditional probabilities of occurrence: P_{FS}

All criteria established was based on fracture fundamentals and the observation of past accident records. The conditional probability, P_{FS}, is relevant for those fragmentation patterns due to deformation forces, one of the final fragments may assume different shapes (e.g., flattened or non-flattened) **[22]**.

Table 06 and **Table 07** list criteria as developed in references **[21]** and **[22]**.

Table 06: Reference Shapes for Fragments [21] [22]

Shape	Description	Geometric Parameters
CE	Cylinder: The fragment is constituted by the entire horizontal or vertical cylindrical vessels.	δ: wall thickness **[m]** ρ: density **[kg·m^{-3}]** l: length **[m]** r: end radius **[m]**
PL	Plate: Flattened shell or pipe section end, or section of a sharp-edged atmospheric equipment.	δ: wall thickness **[m]** ρ: density **[kg·m^{-3}]** l: length **[m]** w: width **[m]**
PT	Tube section: Fragment of a cylindrical shell. If $\xi = 2\pi$ the fragment is a tube.	δ: wall thickness **[m]** ρ: density **[kg·m^{-3}]** l: length **[m]** r: radius **[m]** ξ: arc angle **[rad]**
PTE1	Tube end section #1: Fragment of a cylindrical shell, generated by the propagation of a circumferential and of an axial crack.	δ: wall thickness **[m]** ρ: density **[kg·m^{-3}]** l: length **[m]** r: radius **[m]** ψ: sector angle **[rad]**
PTE2	Tube end section #2: Fragment of a cylindrical shell, generated by the propagation of a circumferential and of an axial crack. If $\psi = 0$ the fragment is a tube end (e.g., generated from a cylindrical vessel by the propagation of a circumferential crack).	δ: wall thickness **[m]** ρ: density **[kg·m^{-3}]** l: length **[m]** r: radius **[m]** ψ: sector angle **[rad]**
SC	Spherical cap: The fragment is a section of a spherical surface, defined by a solid angle γ.	δ: wall thickness **[m]** ρ: density **[kg·m^{-3}]** r: radius **[m]** γ: arc angle **[rad]**
CR	Cone roof: The fragment is a cone, generated by the detachment of the roof of an atmospheric tank.	δ: wall thickness **[m]** ρ: density **[kg·m^{-3}]** h: height **[m]** r: radius **[m]**

***Appendix A.II** graphically illustrates each fragment shape considered.

Table 07: Relationship Between Fragment Patterns and Shapes [21] [22]

Pattern	N_{FT} [-]	Shape	Nº of Shapes; N_{FS} [-]	Angle	P_{FS} [-]
CV1	1	CE	1	-	0.5
		PL	1	-	0.5
CV2	2	PTE2	1	-	1
		PTE2	1	-	0.28
		PL	1	-	0.72
CV3	3	PTE2	2		1
		PTE1	1	$\psi = \pi/8$	0.25
				$\psi = \pi/4$	0.25
				$\psi = 3\pi/8$	0.25
				$\psi = \pi/2$	0.25
CV4	4	PTE2	1	-	1
		PTE1	2	$\psi = \pi/8$	0.25
				$\psi = \pi/4$	0.25
				$\psi = 3\pi/8$	0.25
				$\psi = \pi/2$	0.25
		PL	1	-	1
CV5	3	PTE2	2	-	1
		PL	1	-	1
CV6	4	PTE2	2	-	1
		PTE1	1	$\psi = \pi/8$	0.25
				$\psi = \pi/4$	0.25
				$\psi = 3\pi/8$	0.25
				$\psi = \pi/2$	0.25
		PL	1		1
CV7	$5 \leq N_{FT} \leq 9$	PTE2	2	-	1
		PL	$3 \leq N_{FS} \leq 7$	-	0.5
		PT	$3 \leq N_{FS} \leq 7$	$\xi = \pi/2$	0.125
				$\xi = \pi$	0.125
				$\xi = 3\pi/2$	0.125
				$\xi = 2\pi$	0.125
SV1	$N_{FT} > 1$	SC	*$N_{FS} = -0.425 + 6.115 \cdot 10^{-03} V_V$	-	1
CR1	1	CR	1	-	1

*V_V: spherical vessel volume.

Fragment Drag Factors

The estimation of the expected number of fragments and of fragment reference shapes is the first step towards the calculation of possible fragment trajectories and is needed to estimate the probability of fragment impact on a secondary target. Several models were proposed in the literature for the description of the trajectory of projected fragments. A fundamental approach proposed in reference [27] is considered one of the most widely used for the calculation of the trajectory of projected fragments. This approach is also a suitable method to assess the impact probability of projected fragments. The model is based on the description of the fragment motion considering the fragment acceleration and three types of forces acting on the fragment: gravitational, drag and lift forces. Note that the last two are a function of the shape, mass and orientation of the fragment with respect to the trajectory of its mass center [28]. However, the cited method is complex to implement within the quantitative risk-based assessment framework due to the required prediction of the drag factor of fragments because there is the need to solve differential balance equations via numerical methods.

Based on these needs a general approach based on fragment patterns was developed to estimate the fragment drag factors [22], which is a key parameter to be considered for estimating the fragment trajectory.

Gubinelli and Cozzani [22] developed simplified analytical functions for the drag factors of the reference shapes illustrated in the previous section, based on few geometrical parameters of the vessel undergoing fragmentation. The authors considered a discrete distribution of values of arc angle (ξ) for **PT** shapes and of sector angle (ψ) for **PTE1** and **PTE2** shapes and different simplified drag factor functions were obtained for each value defined. A uniform probability distribution was assumed for each of the values considered. In coherence with the results coming from past accident analysis that did not evidence any preferential value of these mentioned angles [22]. The simplified equations are listed in **Table 08** and detailed information on how the simplified equations were derived can be found in reference [22].

Table 08: Simplified Drag Factor Functions [22]

Shape	Drag Factor Simplified Function		Equation ID
CE		$D_F = \dfrac{0.166}{\rho \cdot \delta}$	Equation 06
PL		$D_F = \dfrac{1.17 + 0.41 \cdot \delta}{\rho \cdot \delta}$	Equation 07
PT	$\xi = \pi/2$	$D_F = \dfrac{1}{\rho \cdot \delta} \cdot \left[\dfrac{2.701}{5 - \delta} + 0.205 \cdot \delta \right]$	Equation 08
	$\xi = \pi$	$D_F = \dfrac{1}{\rho \cdot \delta} \cdot \left[\dfrac{1.910}{5 - \delta} + 0.205 \cdot \delta \right]$	Equation 09
	$\xi = 3\pi/2$	$D_F = \dfrac{1}{\rho \cdot \delta} \cdot \left[\dfrac{1.273}{5 - \delta} + 0.205 \cdot \delta \right]$	Equation 10
	$\xi = 2\pi$	$D_F = \dfrac{1}{\rho \cdot \delta} \cdot \left[\dfrac{0.955}{5 - \delta} + 0.205 \cdot \delta \right]$	Equation 11
PTE1	$\psi = \pi/8$	$D_F = \dfrac{0.550}{\rho \cdot \delta}$	Equation 12
	$\psi = \pi/4$	$D_F = \dfrac{0.450}{\rho \cdot \delta}$	Equation 13
	$\psi = 3\pi/8$	$D_F = \dfrac{0.440}{\rho \cdot \delta}$	Equation 14
	$\psi = \pi/2$	$D_F = \dfrac{0.350}{\rho \cdot \delta}$	Equation 15
PTE2		$D_F = \dfrac{0.240}{\rho \cdot \delta}$	Equation 16
SC		$D_F = \dfrac{0.460}{\rho \cdot \delta}$	Equation 17
CR		$D_F = f(r, h, \delta)$	Equation 18

Note that a simplified drag factor function for Cone-Roof Tank fragments was not possible to be derived as detailed input data is required for drag factor estimation.

Fragment Trajectory

The definition of a reference system is a critical step in addressing fragment trajectory. **Figure 01** illustrates a possible impact condition of a fragment with defined mass, shape and initial velocity on a target equipment.
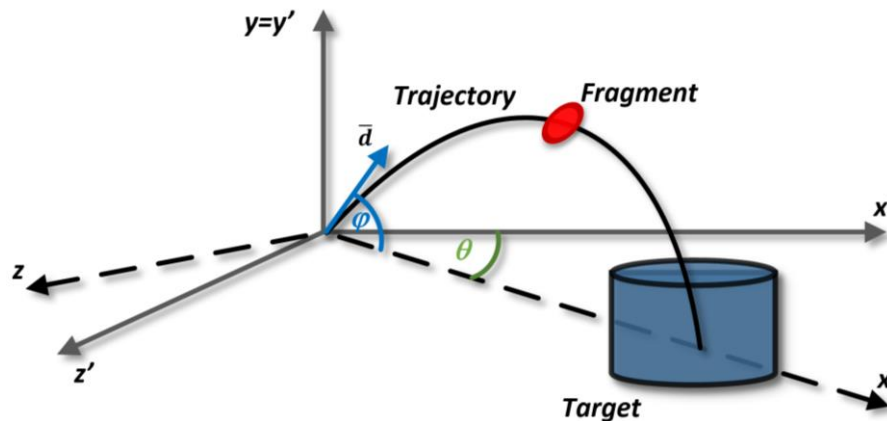

Figure 01: Reference Coordinate System

The initial position of the fragment trajectory is assumed to be the center of the equipment of the explosion, which is the origin point of the absolute reference system $x'y'z'$. A second reference system xyz (with the same origin of the system $x'y'z'$) was defined in which the trajectory of the center of mass belongs to the xy plane. This corresponds to a rotation of the absolute reference system of an angle θ around the y'-axis **[20]**.

The fragment trajectory can be represented on a single xy plane assuming the following approximations: (1) the wind velocity is negligible compared with the fragment velocity; (2) negligible center of mass deviations from the wind and from the possible oscillations caused by fragment rotational movements. Therefore, if the fragment trajectory is analyzed considering the two dimensions (i.e., xy plane), only the elevation angle φ plays a role in the fragment trajectory once the right reference system rotation (angle θ definition) is assumed.

Once the reference system is defined the equations used to characterize the trajectory of a fragment can be derived. The drag factor functions listed in **Table 08** are applicable with a proposed simplified approach intended to describe the trajectory of projected fragments, which is compatible with a quantitative risk-based assessment development. The approach was published in references **[18]** and **[19]** and is based on the simplest equations generally used in mechanics to describe the motion of objects with velocities in the subsonic ranges:

$$\frac{d^2x}{dt^2} + k\left(\frac{dx}{dt}\right)^2 = 0 \qquad\qquad \textbf{Equation 19}$$

$$\frac{d^2y}{dt^2} + (-1)^n k\left(\frac{dy}{dt}\right)^2 + g = 0 \qquad\qquad \textbf{Equation 20}$$

where x and y are the fragment position coordinates at time t, g is the gravitational acceleration, k is thee drag coefficient and n equals 1 for descending trajectory and n equals 2 for ascending trajectory. The following general expression can be used for the calculation of the drag coefficient k as illustrated in **[20] and [28]**:

$$k = a \cdot D_F + b \qquad\qquad \textbf{Equation 21}$$

where a and b are dimensional constants not dependent on the geometrical parameters of the fragment (a equals 0.69 kg·m^{-3} and b equals 3.28E-05 m^{-1}) and D_F is the simplified drag factor function listed in **Table 08** as a function of fragment shape. The term D_F inherently contains information of fragment shape, size and weight.

The analytical solutions of **Equation 19** and **Equation 20** are derived and illustrated in reference **[20]** and are available in **Appendix A.III**.

Note that this approach allows predicts the fragment trajectory given that the characteristics of the type of primary explosion (number of fragments, shapes, sizes, drag factors functions and analytical equations) are defined. Therefore, based on these characteristics and the defining angles θ and φ according to **Figure 01**, the trajectory of the fragment can be predicted.

The following section illustrates criteria for defining the probability of impact of a fragment to a given target. This step requires assigning conditional probabilities on the horizontal (θ) and vertical (φ) angles.

Probability of Fragment Escalation

A general method to assess the probability of fragment impact was developed and illustrated in reference **[20]**. A comparison with data from past accidents and from former studies provided a validation of the model. The probability of fragment impact from a primary event or explosion to a target equipment P_F is expressed as follows:

$$P_F = \sum_{N_{FT}} P_{GEN,F} \cdot P_{IMP,F} \cdot P_{DAM,F}$$

Equation 22

where, the probability P_F corresponds to probabilities of the following event chain:

- $P_{GEN,F}$: Probability of each fragment generated

- $P_{IMP,F}$: The probability of impact on a given target

- $P_{DAM,F}$: Probability of irreversible effects following target impact

- N_{FT}: Expected total number of fragments

Probability of Fragment Generation

($P_{GEN,F}$) quantifies the conditional probability that a fragment with a given shape and mass is formed and projected following the primary event. It can be expressed as follows:

$$P_{GEN,F} = P_{CP} \cdot P_{FP} \cdot P_{FS}$$

Equation 23

- **Table 02** provides guidance for P_{CP} as a function of explosion characteristics

- **Table 05** provides guidance for P_{FP} as a function of fragmentation patterns

- **Table 07** provides guidance for P_{FS} as a function of fragment shapes

Fragment Probability of Impact

The fragment impact occurs when the airborne fragment collides on a given target during its trajectory. The concept of Effective Range Interval (ERI) was introduced in reference **[16]** and considers if impact is possible when the fragment falls within the ERI. Based on the reference system defined in **Figure 01**, two different scenarios can lead to the impact between a flying missile and a target:

- The impact resulting from the missile landing within the Vulnerable Area (VA) of the target ($\Delta\varphi_1$; see **Figure 02**, based on reference **[28]**)

- The impact resulting from the missile colliding with the target object while in flight before reaching the final destination. In this case the target prevents the fragment from landing at a destination beyond the ($\Delta\varphi_2$; see **Figure 02**)
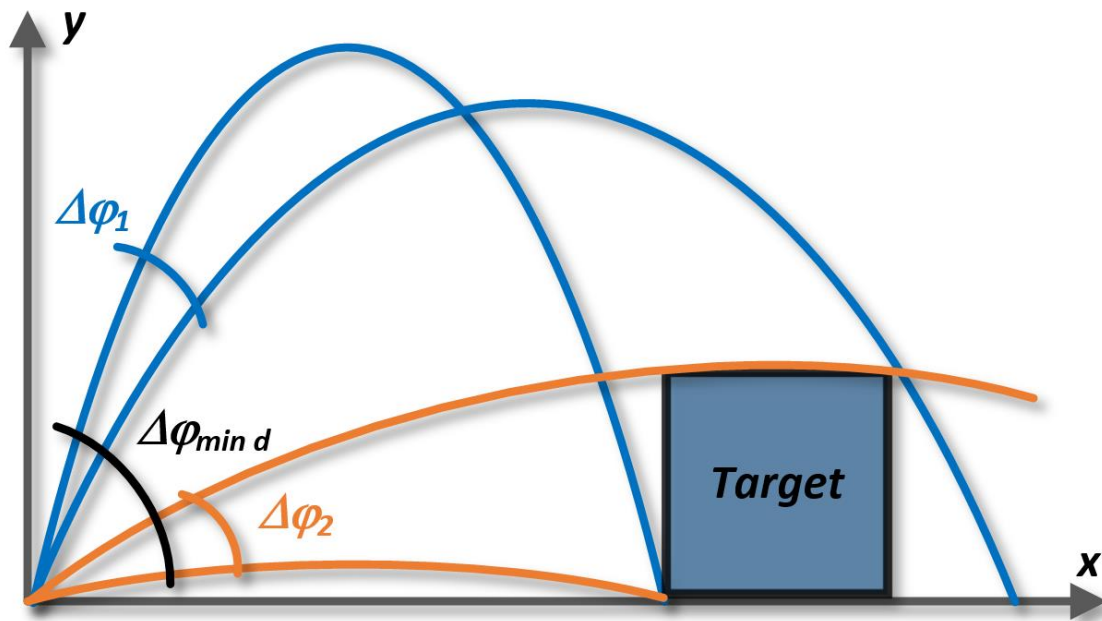
Figure 02: Alternative Impact Conditions of a Fragment - – Vertical Range [16] [28]

The definition of these two impact scenarios accounts for the dimensions of the target, which do not have negligible dimensions in the vertical direction (columns, storage vessels).

Additionally, the target dimensions in the horizontal direction influence the impact probability as illustrated in **Figure 03**, which is based on reference **[28]**.
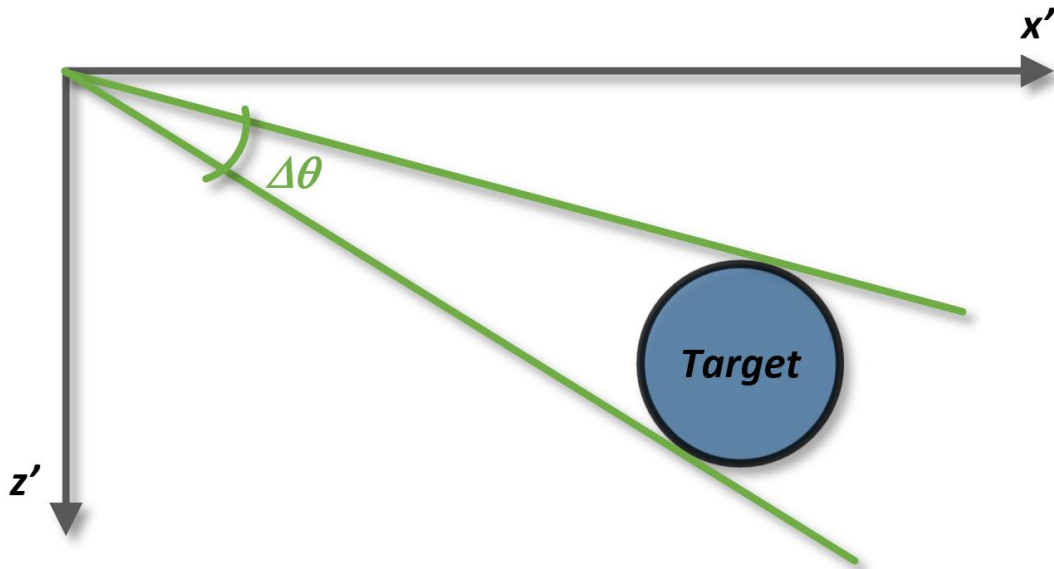
Figure 03: Alternative Impact Conditions of a Fragment – Horizontal Range

Therefore, the impact between the missile and the target is effective for trajectories that have initial angles within limited intervals ($\Delta\theta$ for horizontal angles and $\Delta\varphi_1$ and $\Delta\varphi_2$ for elevation angles). Defining $\Delta\theta$ and $\Delta\varphi$ (where$\Delta\varphi = \Delta\varphi_1 \cup \Delta\varphi_2$) as the intervals identifying all the directional angles θ and φ which result in impact, the total fragment impact probability, F, on the target or on its VA can be estimated. If data for preferential directions for fragment projection are not available, a *uniform probability distribution* was proposed by several authors (**[20]**, **[29]**, **[30]** and **[31]**), which leads to pursued final expression of the fragment impact probability, $P_{IMP,F}$:

$$P_{IMP,F} = \frac{\Delta\theta}{4\pi} \int_{\Delta\varphi} \cos\varphi \, d\varphi$$

Equation 24

Note that **Equation 24** assumes that the φ intervals are not dependent on θ intervals.

The assumption of uniform distribution of the initial direction typically holds only in the case of spherical vessels. As for cylindrical vessel, several studies **[30]**, **[31]** and **[32]** have revealed a preferential direction of projection along the axis of the vessel:

▪ Reference **[32]** indicated that about 50% of the total fragments were projected into one-third of the total area, in arcs of 30⁰ to either side of the vessel's front and rear axial directions.

- Reference **[31]** indicated that about 50% of the total fragments were projected with uniform probability within a horizontal angle of 15⁰ per side from the axis of the vessel. The other 50% of the fragments were projected with uniform probability distribution on the other two angle intervals at the sides of the vessel. For elevation angles, a uniform distribution of probability in the interval [0⁰, 15⁰] was proposed.

- Based on the analysis performed in reference **[30]**, the following criteria is proposed in this paper:

  - Horizontal angles, $\boldsymbol{\theta}$: 60% of the fragments are projected with uniform probability distribution in:

    - $\theta \in [330, 30] \cup [150, 210]$; i.e., $\theta \in [11\pi/6, \pi/6] \cup [5\pi/6, 7\pi/6]$

  - Elevation angles, $\boldsymbol{\varphi}$: uniform probability distribution over the full range of:

    - $\varphi \in [-90, 90]$; i.e., $\varphi \in [-\pi/2, \pi/2]$

Fragment Probability of Damage

A fragment can cause damage to several targets by striking and penetrating, or rebounding without penetrating. The term penetration usually is defined as the event that the fragment disrupts or displaces some of the target material during impact, but does not pass through the target; and it may or may not remain lodged in the target. If the missile passes entirely through, the target is said to have been perforated **[27]**.

The damage by fragment impact more frequently analyzed in the literature is the penetration of the target. The models available for fragment penetration in metal targets are mostly based on the fitting of experimental data, usually from tests on missiles with sizes smaller than the typical fragments originated by vessel failure.

The fragment penetration models provide the evaluation of a penetration parameter in function of the missile and target characteristics. Depending on the model, the penetration parameter can be defined as one of the following:

- The minimum kinetic energy of the missile resulting in target perforation for a given material thickness

- The maximum thickness of penetration

- The minimum missile impact velocity for target perforation of a given material thickness

- The missile impact velocity resulting in 50% probability for target perforation of a given material thickness

Under the assumption that surface effects do not influence penetration (which is reasonable for targets which are thin compared to the missile size), all the literature correlations can be mathematically configured to express the maximum thickness that can be perforated by a fragment **[28]**.

Though several models are available to calculate fragment penetration on a given target, no criteria are available to estimate the actual damage probability **[28]**. In absence of reliable damage models, a common conservative criterion, is to assume a unit value for the damage probability if impact occurs **[29]**:

$$P_{DAM,F} = 1$$

Equation 25

Frequency of Occurrence of Domino Effect Triggered by Fragments Impact

The frequency of a domino event caused by the impact of fragments generated in a primary accident on a given secondary target, (f_F) may be expressed as:

$$f_F = f_P \cdot P_F = f_P \cdot \sum_{N_{FT}} P_{GEN,F} \cdot P_{IMP,F} \cdot P_{DAM,F}$$

Equation 26

where:

P_F: Probability of fragment escalation

f_P: Frequency of the primary event, which is obtained by using either generic failure data, or engineering tools that perform frequency analysis, such as Fault Tree Analysis.

Detailed information on how to estimate frequencies of primary events (Loss Of Containment scenarios – LOCs) can be found in **[33]**.

Application of the Proposed Risk-Based Approach

The proposed missile impact domino effect analysis requires completing a robust quantitative risk-based assessment based on criteria in references **[5]**, **[6]**, **[33]**, **[34]**, **[35]**, **[36]** and **[37]**. The results from the quantitative risk-based assessment are considered the starting point for developing the proposed analysis which provides key explosion data. The following are a step-by-step procedure for conducting the proposed domino effect analysis.

Step 1. Identification of all vessel burst scenarios and collection of relevant information:

- Primary event frequency of occurrence (f_P)

- Type of the explosion according to **Table 01**

- Vessel features: Shape (i.e., **CV**, **SC**, or **CR**), material density (ρ), dimensions (length l, width w, height h, radius r, depending on vessel shape), wall thickness δ and associated vessel volume V_V, vessel mass M_V

- Parameters at TTF: Available internal energy E_I, gas speed of sound a and rupture pressure, P

Step 2. Selection of vessel burst scenario (i.e., primary explosion):

- Based on the explosion type, the probability of fragment generation P_{CP} can be established (see **Table 02**). Based on vessel shape, the following parameters can be acquired:

  o Fragment initial velocity model to be used (see **Table 03**)

  o Identification of applicable fragment patterns (**CV1**, **CV2**, **CV3**, **CV4**, **CV5**, **CV6**, **CV7**, **SV1**, **CR1**) and associated probability of fragmentation pattern P_{FP} (see **Table 05**)

  o Identification of the expected total number of fragments N_{FT}, fragment shapes (**CE**, **PL**, **PT**, **PTE1**, **PTE2**, **SC**, **CR**) and expected total number of fragments with the same shape N_{FS}. Additionally, the conditional probability of fragment shape P_{FS} can be identified (see **Table 07**)

Step 3. Selection of target equipment to be analyzed:

- Estimation of the impact distance between target and primary explosion

Step 4. Selection of first applicable fragment pattern.

Step 5. Selection of first fragment shape from the given fragment pattern:

- Estimation of drag factor functions (see **Table 08**)

- Estimation of probability of fragment generation $P_{GEN,F}$ (**Equation 23**)

- Iterative computational solution of trajectory equations (**Equation 19**, **Equation 20**, **Equation 21** and **Appendix III**) using multiple combinations of horizontal and vertical angles that satisfy the separation distance between the primary explosion and the target.

- Estimation of the probability of impact $P_{IMP,F}$ (**Equation 24**) based on horizontal and vertical angle combinations that satisfy the distance between the primary explosion and target and the criteria on preferential direction of projection based on reference **[30]**.

- Estimation of the probability of damage $P_{DAM,F}$ (**Equation 25**)

First Iteration. The iteration is repeated per all shapes for a given fragment pattern (**Step 5** iteration).

Second Iteration. The iteration is repeated per all patterns for a given primary explosion (**Step 4** iteration).

Step 6. Consideration of the frequency of occurrence of domino effect (based on **Step 1**).

- Estimation of the frequency of domino effect triggered by fragment impacts using **Equation 26**

Third Iteration. Analysis of all targets of interest. The iteration is repeated per all targets to be covered for potential missile impact from the selected primary explosion (**Step 3** to **Step 6** iteration).

Fourth Iteration. Analysis of all vessel burst scenarios. The iteration is repeated per all primary explosions identified during the quantitative risk-based assessment (**Step 2** to **Step 6** iteration).

Figure 04 graphically illustrates the procedure via a simplified flowchart.

The illustrated step-by-step procedure can be applied for very specific target locations and also for ALL locations in a map area (process facility boundaries and neighborhood). It is conducted during the generation of risk contours for toxicity, overpressure and thermal radiation hazards in a quantitative risk-based analysis. In fact, the main goal of the proposed domino effect analysis is to generate the "Missile Impact Risk Contours" (i.e., isorisk contours) by risk-mapping the entire area of interest.

The estimation of missile impact risk contours is a substantial effort given the multitude iterations required to cover all primary scenarios and all locations defined in the risk map. However, recent powerful computational capabilities and enhanced routines allow optimizing the execution of the proposed risk-based approach by minimizing time and investment.

Estimating the missile impact risk contours results in a complete quantitative risk-based assessment for a given process facility.

While most of current risk assessments consider the overall risk by cumulating the risk levels of toxicity, overpressure and thermal radiation hazards, the incorporation of the missile impact risk results from the proposed domino effect analysis provides the most comprehensive quantitative risk-based assessment.
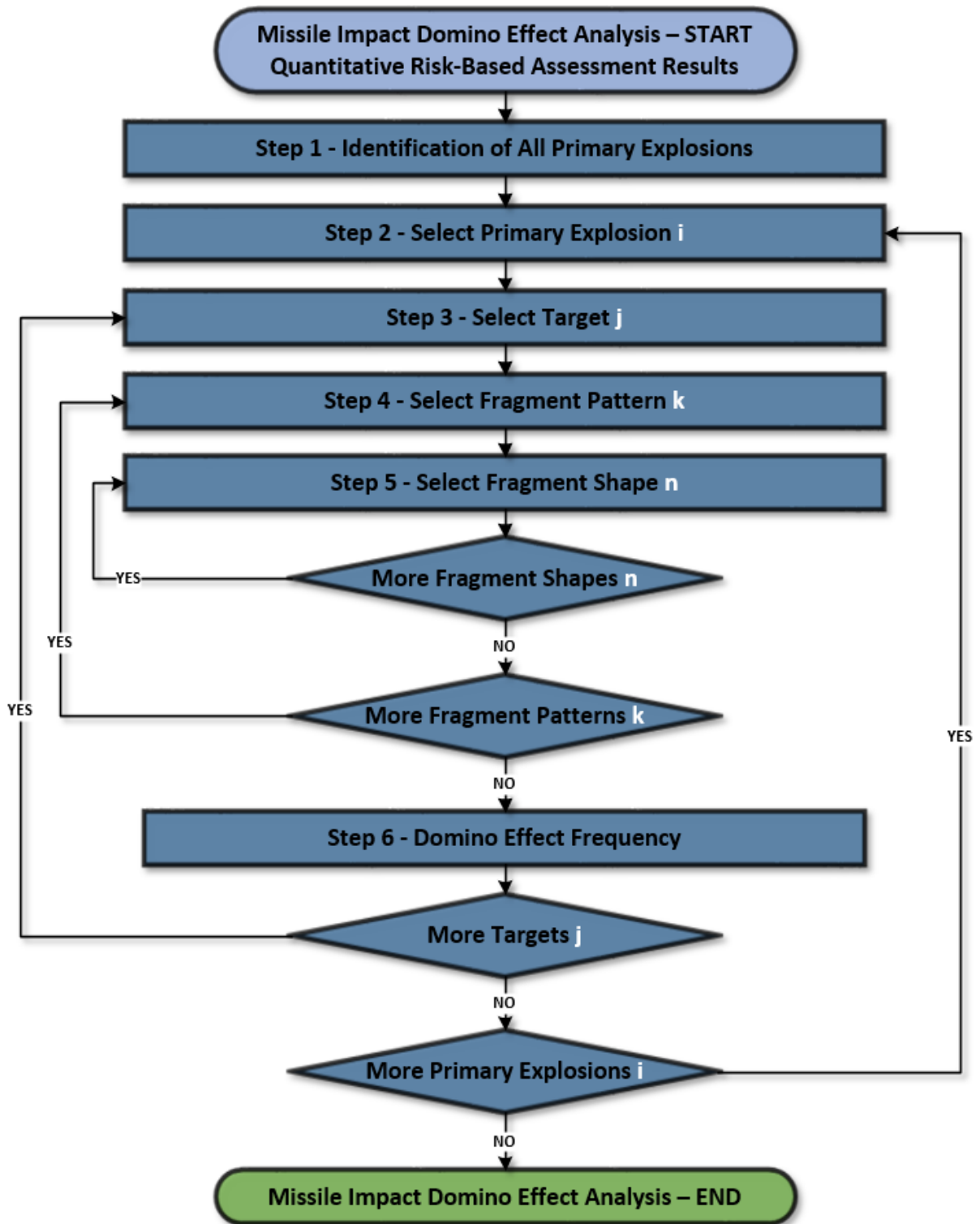
Figure 04: Proposed Missile Impact Domino Effect Procedure – Simplified Flowchart

Conclusion

This paper presents a risk-based missile impact domino effect assessment that addresses fragment projection following vessel burst scenarios. The proposed approach strictly follows criteria and knowledge developed in references **[20]**, **[21]**, **[22]** and **[23]**. The analysis of a database reporting data on more than 143 vessel fragmentation events allowed:

- The identification of a limited number of fragment reference shapes

- The correlation of fragment reference shapes to the credible vessel fragmentation patterns allows for calculation of the expected number and reference shape of fragments generated

- Simplified functions for drag factor calculation were developed, based on few geometrical parameters of the vessel undergoing the fragmentation event

The probabilistic models for the expected shape and number of fragments with the simplified drag factor functions constitute an important input to analyze the possible fragment trajectories in the quantitative risk-based assessment framework.

Estimating the missile impact risk contours results in a complete quantitative risk-based assessment for a given process facility. While most of current risk assessments consider the overall risk by cumulating the risk levels of toxicity, overpressure and thermal radiation hazards, the incorporation of the missile impact risk results from the proposed domino effect analysis provides the most comprehensive quantitative risk-based assessment.

References

[1] Necci, A., Cozzani, V., Spadoni, G., Khan, F., 2015. "Assessment of Domino Effect – State of the Art and Research Needs". Reliability Engineering and System Safety. Elsevier.

[2] Dunjó, J., Amorós, M., Prophet, N., Gorski, G., 2016. "Risk-Based Approach – Fires. Introduction to Fires and Dynamic Thermal Stress Analysis". An ioMosaic White Paper, ioMosaic Corporation.

[3] Dunjó, J., Amorós, M., Prophet, N., Gorski, G., 2016. "Risk-Based Approach – Domino Effect and Escalation Triggered by Fires. Combining Dynamic Thermal Stress Analysis and Wall Segmentation Approach". An ioMosaic White Paper, ioMosaic Corporation.

[4] Melhem, G. A., 2015. "Advanced Consequence Analysis; Fluid Flow, Emergency Relief Systems Design, Thermal Hazards Assessment, Emission, Dispersion, Fire and Explosion Dynamics." ioMosaic Corporation.

[5] Dunjó, J., Amorós, M., Prophet, N., Gorski, G., 2016. "Risk-Based Approach – Consequence Analysis. An Introduction to Consequence Modeling and Identification of Outcomes from Loss of Containment Scenarios". An ioMosaic White Paper, ioMosaic Corporation.

[6] Dunjó, J., Amorós, M., Prophet, N., Gorski, G., 2016. "Risk-Based Approach – Damage Criteria. An Overview of the State-of-the-Art Damage Criteria for People and Structures". An ioMosaic White Paper, ioMosaic Corporation.

[7] Dunjó, J., Amorós, M., Prophet, N., Gorski, G., 2016. "Risk-Based Approach – Explosions and Blast Loading. Introduction to Explosions and Structure Blast Loading Phenomena". An ioMosaic White Paper, ioMosaic Corporation.

[8] Dunjó, J., Amorós, M., Prophet, N., Gorski, G., 2016. "Risk-Based Approach – Facility Siting Addressing Explosions Impacting Process Plant Permanent and Portable Buildings. Combining Exceedance Curves, Structural Response and Human Vulnerability Criteria". An ioMosaic White Paper, ioMosaic Corporation.

[9] Dunjó, J., Amorós, M., Prophet, N., Gorski, G., 2016. "Risk-Based Approach – Domino Effect and Escalation Triggered by Explosions. Combining Exceedance Curves and Overpressure Threshold Criteria". An ioMosaic White Paper, ioMosaic Corporation.

[10] Dunjó, J., Amorós, M., Prophet, N., Gorski, G., 2016. "Risk-Based Approach – Domino Effect and Escalation Triggered by Explosions. Combining Exceedance Curves, Single Degree of Freedom and Pressure-Impulse Diagrams.". An ioMosaic White Paper, ioMosaic Corporation.

[11] Dunjó, J., Amorós, M., Prophet, N., Gorski, G., 2016. "Risk-Based Approach - Facility Siting Addressing Fires Impacting Process Plant Permanent and Portable Buildings. Combining Exceedance Curves and Human Vulnerability Criteria". An ioMosaic White Paper, ioMosaic Corporation.

[12] Dunjó, J., Amorós, M., Prophet, N., Gorski, G., 2016. "Risk-Based Approach – Domino Effect and Escalation Triggered by Fires. Combining Exceedance Curves and Time to Failure (TTF) Simplified Methodologies". An ioMosaic White Paper, ioMosaic Corporation.

[13] Dunjó, J., Amorós, M., Prophet, N., Gorski, G., 2016. "Risk-Based Approach – Hazardous Vapor Cloud Dispersions. An Introduction to Dispersion Modeling". An ioMosaic White Paper, ioMosaic Corporation.

[14] Dunjó, J., Amorós, M., Prophet, N., Gorski, G., 2016. "Risk-Based Approach – Facility Siting Addressing Hazardous Vapor Cloud Dispersions Impacting Process Plant Permanent and Portable Buildings. Combining Exceedance Curves and Human Vulnerability Criteria". An ioMosaic White Paper, ioMosaic Corporation.

[15] CCPS, 1994. "Guidelines for Evaluating the Characteristics of Vapor Cloud Explosions, Flash Fires and BLEVEs". Center for Chemical Process Safety of the American Institute of Chemical Engineers. New York, New York.

[16] Scilly, N.F., Crowter, J.H., 1992. "Methodology for Predicting Domino Effects from Pressure Vessel". International Conference on Hazard Identification and Risk Analysis, Human Factors and Human Reliability in Process Safety.

[17] Baum, M, R., 2001. "The Velocity of Large Missiles from Axial Rupture of Gas Pressurized Cylindrical Vessels". Journal of Loss Prevention in the Process Industries, 14:199‑203.

[18] Hauptmanns, U., 2001. "A Monte Carlo-Based Procedure for Treating the Flight of Missiles form Tank Explosions". Probab. Eng. Mech., 2001; 16:307‑312.

[19] Hauptmanns, U., 2001. "A Procedure for Analyzing the Flight of Missiles from Explosions of Cylindrical Vessels". Journal of Loss Prevention in the Process Industries, 14:395‑402.

[20] Gubinelli, G., Zanelli, S., Cozzani, V., 2004. "A Simplified Model for the Assessment of the Impact Probability of Fragments". Journal of Hazardous Materials, 116:175-187.

[21] Gubinelli, G., Cozzani, V., 2009. "Assessment of Missile Hazard: Reference Fragmentation Patterns of Process Equipment". Journal of Hazardous Materials, 163, 1008-1018.

[22] Gubinelli, G., Cozzani, V., 2009. "The Assessment of Missile Hazard: Evaluation of Fragment Number and Drag Factors." Journal of Hazardous Materials, 161, 439-449.

[23] Tugnoli, A., Gubinelli, G., Landucci, G., Cozzani, V., 2014. "Assessment of Fragment Projection Hazard: Probability Distributions for the Initial Direction of Fragments". Journal of Hazardous Materials, 279:418-427.

[24] Tugnoli, A., Milazzo, M.F., Landucci, G., Cozzani, V., Maschio, G., 2014. "Assessment of the Hazard Due to Fragment Projection: A Case-Study", Journal of Loss Prevention in the Process Industries 2014b; 28:36-46.

[25] Nguyen, Q.B., Mebarki, A, Ami Saada, R., Mercier ,F., Reimeringer, M., 2009. "Integrated Probabilistic Framework for Domino Effect and Risk Analysis". Advances in Engineering Software 40:892‑901.

[26] Zhang, X., Chen, G., 2009. "The Analysis of Domino Effect Impact Probability Triggered by Fragments". Safety Science, 47, 1026-1032.

[27] Baker, W.E., Cox, P.A., Westine, P.S., Kulesz, J.J., Strehlow, R. A., 1983. "Explosion Hazards and Evaluation". Elsevier Scientific Publishing Company. ISBN 0-444-42094-0 (Vol.5).

[28] Reniers, G., Cozzani, V., 2013. "Domino Effects in the Process Industries – Modeling, Prevention and Managing". Elsevier, Amsterdam ISBN: 978-0-444-54323-0.

[29] Mannan, S., 2005. "Lees' Loss Prevention in the Process Industries". Third Edition. Elsevier, Oxford, United Kingdom.

[30] Mébarki, A., Mercier, F., Nguyen, Q.B., Saada, R.A., 2009. "Structural Fragments and Explosions in Industrial Facilities. Part I: Probabilistic Description of the Source Terms". Journal of Loss Prevention in the Process Industries 21, 518-527.

[31] Pula, R., Khan, F.I., Veitch, B., Amyotte, P.R., 2007. "A Model for Estimating the Probability of Missile Impact: Missiles Originating from Bursting Horizontal Cylindrical Vessels". Process Safety Progress, 26 (2), 129-139.

[32] Holden, P.L., Reeves, A.B., 1985. "Fragment Hazards from Failures of Pressurized Liquefied Gas Vessels". IChemE Symposium Series 93, 205.

[33] Dunjó, J., Amorós, M., Prophet, N., Gorski, G., 2016. "Risk-Based Approach – Frequency Analysis. Estimating Frequencies of Occurrence and Conditional Probabilities of Loss of Containment Scenarios". An ioMosaic White Paper, ioMosaic Corporation.

[34] Amorós, M., Dunjó, J., Prophet, N., Gorski, G., 2016. "Quantitative Risk-Based Assessment. Foundation for Process Safety and Loss Prevention". An ioMosaic White Paper, ioMosaic Corporation.

[35] Dunjó, J., Amorós, M., Prophet, N., Gorski, G., 2016. "Risk-Based Approach – Hazard Identification. Guidance for Identifying Loss of Containment Scenarios". An ioMosaic White Paper, ioMosaic Corporation.

[36] Amorós, M., Dunjó, J., Prophet, N., Gorski, G., 2016. "Risk-Based Approach – Risk Evaluation. Tools for Risk Characterization". An ioMosaic White Paper, ioMosaic Corporation.

[37] Dunjó, J., Amorós, M., Prophet, N., Gorski, G., 2016. "Risk-Based Approach –Risk Tolerability Criteria. An Overview of Worldwide Risk Tolerability Criteria for Chemical Process Industries". An ioMosaic White Paper, ioMosaic Corporation.
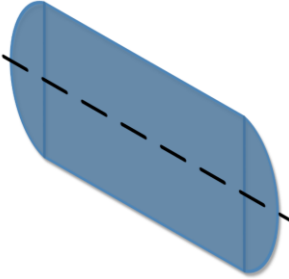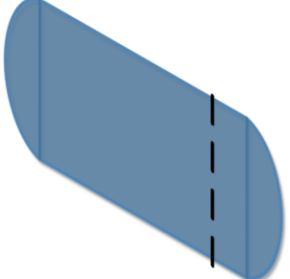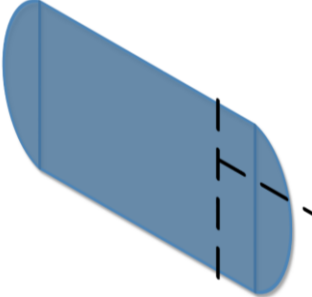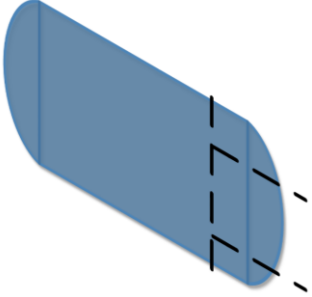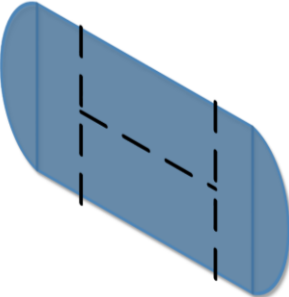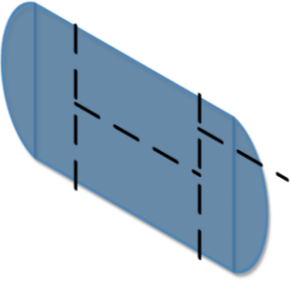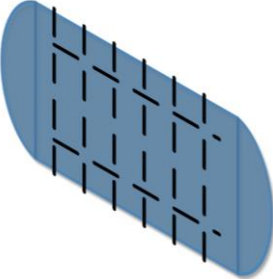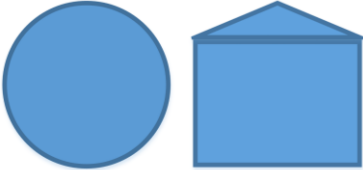
Appendix I: Graphical Representation of Reference Fragmentation Patterns

The graphical representation of the different reference fragmentation patterns illustrated in Table A.I are based on Table 6.5 from reference **[28]**. Equivalent illustrations can be found in references **[21]** and **[22]**.

Table A.I: Graphical Representation of Reference Fragmentation Patterns

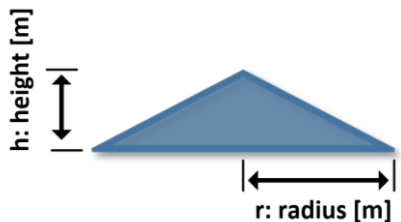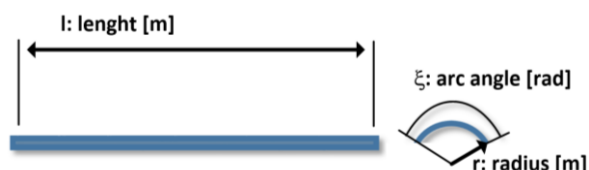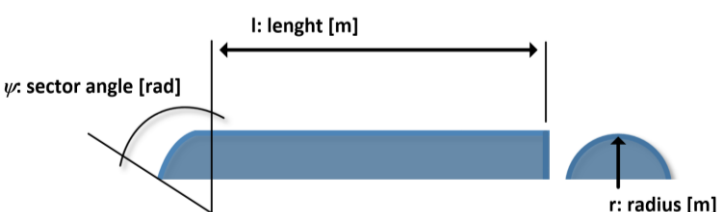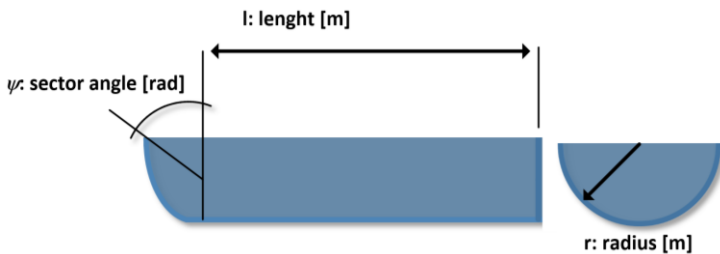| Pattern	Graphical Illustration	Pattern	Graphical Illustration
CV1		CV2	
CV3		CV4	
CV5		CV6	
CV7		SV1 CR1	
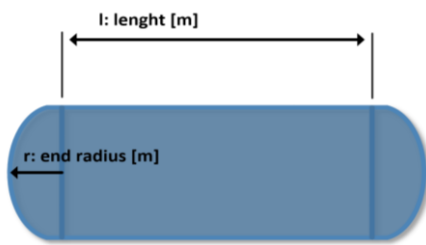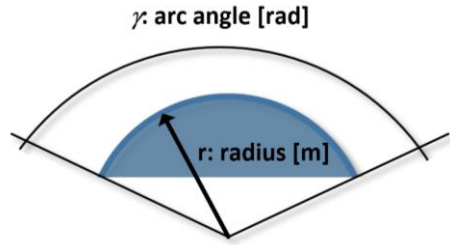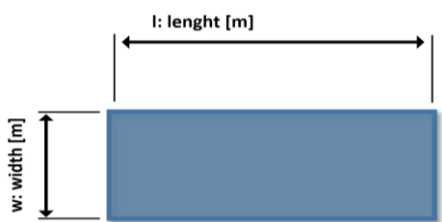
CV: Cylindrical Vessel; **SV**: Spherical Vessel; **CR**: Cone-Roof Tank.

Appendix II: Graphical Representation of Reference Fragment Shapes

The graphical representation of the different reference fragment shapes illustrated in Table A.II are based on Table 6.6 from reference **[28]**. Equivalent illustrations can be found in references **[21]** and **[22]**.

Table A.II: Graphical Representation of Reference Fragment Shapes

Shape	Graphical Illustration	Shape	Graphical Illustration
CE		SC	
PL		CR	
PT			
PTE1			
PTE2			

CE: Cylinder; **PL**: Plate; **PT**: Tube Section; **PTE1**: Tube end section – Shape #1; **PTE2**: Tube end section – Shape #2; **SC**: Spherical Cap; **CR**: Cone Roof

Appendix III: Analytical Expression of Fragment Trajectory

Equations illustrated in **Appendix III** represent the analytical solutions of **Equation 19** and **Equation 20**.

$$\frac{d^2x}{dt^2} + k\left(\frac{dx}{dt}\right)^2 = 0 \qquad\qquad \textbf{Equation 19}$$

$$\frac{d^2y}{dt^2} + (-1)^n k\left(\frac{dy}{dt}\right)^2 + g = 0 \qquad\qquad \textbf{Equation 20}$$

where x and y are the coordinates of the position of the fragment at time t, g is the gravitational acceleration, k is de drag coefficient and n equals 1 in the descending part and n equals 2 in the ascending part of the trajectory,.

Note that φ is the angle used to define the initial direction of the fragment projection in the vertical plane.

Appendix III contents are based on reference [20].

Solution of **Equation 19**:

$$\frac{dx}{dt} = \frac{u\cos(\varphi)}{1 + k \cdot t \cdot u\cos(\varphi)}$$

Equation A.III.01

$$x(t) = \frac{1}{k} \cdot \ln[1 + k \cdot t \cdot u\cos(\varphi)]$$

Equation A.III.02

Solution of **Equation 20**; ascending part:

$$\frac{dy}{dt} = \frac{\tan\left\{\tan^{-1}\left[\sqrt{\frac{k}{g}} \cdot u\sin(\varphi)\right] - \sqrt{\frac{k}{g}} \cdot g \cdot t\right\}}{\sqrt{\frac{k}{g}}}$$

Equation A.III.03

$$y(t) = -\frac{1}{2k} \cdot \ln\left[\frac{\frac{k}{g} \cdot \left(\frac{dy}{dt}\right)^2 + 1}{\frac{k}{g} \cdot [u\sin(\varphi)]^2 + 1}\right]$$

Equation A.III.04

Solution of **Equation 20**; descending part:

$$\frac{dy}{dt} = \frac{1 - exp\left\{\left(\frac{2k}{\sqrt{\frac{k}{g}}}\right) \cdot t - 2 \cdot \tan^{-1}\left[\sqrt{\frac{k}{g}} \cdot u\sin(\varphi)\right]\right\}}{\sqrt{\frac{k}{g}} \cdot \left[1 + exp\left\{\left(\frac{2k}{\sqrt{\frac{k}{g}}}\right) \cdot t - 2 \cdot \tan^{-1}\left[\sqrt{\frac{k}{g}} \cdot u\sin(\varphi)\right]\right\}\right]}$$

Equation A.III.05

$$y(t) = \frac{1}{2k} \cdot \ln\left[\frac{k}{g} \cdot [u\sin(\varphi)]^2 + 1\right] + \frac{1}{2k} \cdot \ln\left[1 - \frac{k}{g} \cdot \left(\frac{dy}{dt}\right)^2\right]$$

Equation A.III.06